

Third-order spontaneous parametric downconversion in thin optical fibers as a photon-triplet source

María Corona,^{1,2,*} Karina Garay-Palmett,¹ and Alfred B. U'Ren¹

¹*Instituto de Ciencias Nucleares, Universidad Nacional Autónoma de México, apdo. postal 70-543, México 04510 DF*

²*Departamento de Óptica, Centro de Investigación Científica y de Educación Superior de Ensenada, Apartado Postal 2732, Ensenada, BC 22860, México*

*Corresponding author: maria.corona@nucleares.unam.mx

(Dated: November 5, 2018)

We study the third-order spontaneous parametric downconversion (TOSDPC) process, as a means to generate entangled photon triplets. Specifically, we consider thin optical fibers as the nonlinear medium to be used as the basis for TOSDPC, in configurations where phasematching is attained through the use of different fiber transverse modes. Our analysis in this paper, which follows from our earlier paper Opt. Lett. **36**, 190–192 (2011), aims to supply experimentalists with the details required in order to design a TOSDPC photon-triplet source. Specifically, our analysis focuses on the photon triplet state, on the rate of emission, and on the TOSDPC phasematching characteristics, for the cases of frequency-degenerate and frequency non-degenerate TOSDPC.

PACS numbers: 42.50.-p, 42.65.Lm

I. INTRODUCTION

The generation of entangled photon multiplets represents an important goal in quantum optics, as a resource for fundamental tests of quantum mechanics as well as for the implementation of quantum-enhanced technologies. A large number of experiments from the last few decades have exploited entangled photon *pairs* generated by the process of spontaneous parametric downconversion (SPDC) in second-order non-linear crystals [1]. Recently, the process of spontaneous four wave mixing (SFWM) based on the third-order nonlinearity of optical fibers has emerged as a viable alternative to SPDC for the generation of photon pairs [2]. However, the generation of entangled photon *triplets*, and of higher-order entangled photon multiplets, faces acute technological challenges.

The motivation which served as starting point for the present work is that in principle the same third order non-linearity in fused silica optical fibers which is responsible for the SFWM process also permits a different process: third-order spontaneous parametric downconversion (TOSDPC) [3–8]. While in the SFWM process, two pump photons are jointly annihilated in order to generate a photon *pair*, in the TOSDPC process a single pump photon is annihilated in order to generate a photon *triplet*. TOSDPC may be differentiated from other approaches based on nonlinear optics for the generation of photon triplets, by the fact that the three photons in a given triplet are derived from a single quantum-mechanical event. The prospect of efficient generation of photon triplets is exciting on a number of fronts. On the one hand, it naturally leads to the possibility of heralded emission of photon pairs [9–11]. On the other hand, it leads to the possibility of direct generation of Greenberger-Horne-Zeilinger (GHZ) polarization-entangled states [12, 13], without resorting to postselection. In addition, if the photon triplets are emitted in a single transverse-mode environment they exhibit factora-

bility in transverse momentum, but can exhibit spectral entanglement. Such three-partite entanglement in a continuous degree of freedom is a potentially important, yet largely unexplored topic.

A number of approaches for the generation of photon triplets have been proposed including: i) triexcitonic decay in quantum dots [14], ii) combined, or cascaded, second-order nonlinear processes [15–17], and iii) approximate photon triplets formed by SPDC photon pairs together with an attenuated coherent state [18]. Of these approaches, those that have been experimentally demonstrated lead to very low photon-triplet detection rates. Recently, we have proposed a specific technique for the generation of photon triplets based on the TOSDPC process in thin optical fibers and relying on multiple transverse fiber modes [19]. As will be discussed below, the emission rates predicted for a source based on our proposal are likewise low. However, future advances in optical fiber technology, specifically in the form of highly-nonlinear fibers, photonic crystal fibers, and tapered fibers may significantly increase the emitted flux attainable through our proposal.

The purpose of this paper is to explore the theory behind our proposal for TOSDPC photon-triplet sources. In particular, we focus on the photon-triplet state, on the rate of emission, and on the TOSDPC phasematching characteristics of thin optical fibers. In order to make our analysis as general as possible, we include both frequency-degenerate and frequency non-degenerate TOSDPC, as well as both the monochromatic- and pulsed-pumped regimes.

II. DERIVATION OF THE PHOTON-TRIPLET QUANTUM STATE

In this paper we study the process of third-order spontaneous parametric downconversion (TOSDPC) in opti-

cal fibers, in which nonlinear phenomena originate from the third-order electrical susceptibility $\chi^{(3)}$. In this process, individual photons from the pump mode (p), may be annihilated giving rise to the emission of a photon triplet. Borrowing from second-order spontaneous parametric downconversion terminology, we refer to the three emission modes as signal-1 (r), signal-2 (s), and idler (i). We restrict our analysis to configurations for which the three TOSPDG photons are generated in the same transverse fiber mode, and where all four fields are co-polarized (with linear polarization along the x -axis) propagating in the same direction along the fiber (which defines the z -axis).

It can be shown that the TOSPDG process is governed by the following Hamiltonian

$$\hat{H}(t) = \frac{3}{4}\epsilon_0\chi^{(3)} \times \int dV \hat{E}_p^{(+)}(\mathbf{r}, t) \hat{E}_r^{(-)}(\mathbf{r}, t) \hat{E}_s^{(-)}(\mathbf{r}, t) \hat{E}_i^{(-)}(\mathbf{r}, t), \quad (1)$$

in terms of the positive-frequency and negative-frequency parts of the electric field operator (denoted by $(+)$ / $(-)$ superscripts) for each of the modes, labeled as $\mu = p, r, s, i$. In Eq. (1), ϵ_0 represents the vacuum electric susceptibility, and the integral is evaluated over the nonlinear medium volume illuminated by the pump field. $E_\mu^{(+)}(\mathbf{r}, t)$ (with $\mu = r, s, i$) may be written as

$$\hat{E}^{(+)}(\mathbf{r}, t) = iA(x, y)\sqrt{\delta k} \sum_k \ell(\omega) \exp[i(kz - \omega t)] \hat{a}(k), \quad (2)$$

where $\hat{a}(k)$ is the wavenumber-dependent annihilation operator associated with the propagation mode in the fiber, and $\delta k = 2\pi/L_Q$ is the mode spacing defined in terms of the quantization length L_Q . $A(x, y)$ represents the transverse spatial distribution of the field, which is approximated to be frequency-independent within the bandwidth of the generated wave-packets, and is normalized so that $\int \int |A(x, y)|^2 dx dy = 1$. In Eq. (2) the function $\ell[\omega(k)]$ is given as

$$\ell(\omega) = \sqrt{\frac{\hbar\omega}{\pi\epsilon_0 n^2(\omega)}}, \quad (3)$$

where $n(\omega)$ is the refractive index of the medium and \hbar is Planck's constant.

For the analysis presented here, we describe the pump mode as a classical field, expressed in terms of its Fourier components as

$$E_p^{(+)}(\mathbf{r}, t) = A_0 A_p(x, y) \int d\omega_p \alpha(\omega_p) \exp[i(k_p(\omega_p)z - \omega_p t)], \quad (4)$$

in terms of the pump-mode amplitude A_0 , and the pump transverse distribution in the fiber $A_p(x, y)$, normalized so that $\int \int |A_p(x, y)|^2 dx dy = 1$, and approximated to be frequency-independent within the pump bandwidth. In Eq. (4), the function $\alpha(\omega_p)$ is the pump spectral amplitude (PSA), with normalization $\int |\alpha(\omega)|^2 d\omega = 1$. It can be shown that A_0 is related to pump peak power P through

$$A_0 = \sqrt{\frac{2P}{\epsilon_0 c n_p |\int d\omega_p \alpha(\omega_p)|^2}}, \quad (5)$$

where $n_p \equiv n(\omega_{p0})$; ω_{p0} is the pump carrier frequency.

By replacing Eqs. (2) and (4) into Eq. (1), and following a standard perturbative approach [20], it can be shown that the state produced by third-order spontaneous parametric down conversion is $|\Psi\rangle = |0\rangle_r |0\rangle_s |0\rangle_i + \xi |\Psi_3\rangle$, written in terms of the three-photon component of the state $|\Psi_3\rangle$

$$|\Psi_3\rangle = \sum_{k_r} \sum_{k_s} \sum_{k_i} G_k(k_r, k_s, k_i) \times \hat{a}^\dagger(k_r) \hat{a}^\dagger(k_s) \hat{a}^\dagger(k_i) |0\rangle_r |0\rangle_s |0\rangle_i, \quad (6)$$

where ξ , related to the conversion efficiency, is given by

$$\xi = i \frac{3\epsilon_0 \chi^{(3)} (2\pi) A_0 (\delta k)^{3/2} L}{4\hbar} \times \int dx \int dy A_p(x, y) A_r^*(x, y) A_s^*(x, y) A_i^*(x, y). \quad (7)$$

In Eq. (6), $G_k(k_r, k_s, k_i)$ is the wavenumber joint amplitude. Writing this function in terms of frequencies leads to $G(\omega_r, \omega_s, \omega_i) = \ell(\omega_r) \ell(\omega_s) \ell(\omega_i) F(\omega_r, \omega_s, \omega_i)$. The function $\ell(\omega)$ has a slow dependence on frequency [see Eq. (3)] over the spectral range of interest. If this dependence is neglected, the photon-triplet spectral properties are fully determined by the function $F(\omega_r, \omega_s, \omega_i)$, which from this point onwards we refer to as the joint spectral amplitude. It can be shown that this function can be written in terms of the pump spectral amplitude (PSA) $\alpha(\omega)$, and the phasematching function (PM) $\phi(\omega_r, \omega_s, \omega_i)$ as

$$F(\omega_r, \omega_s, \omega_i) = \alpha(\omega_r + \omega_s + \omega_i) \phi(\omega_r, \omega_s, \omega_i), \quad (8)$$

with

$$\phi(\omega_r, \omega_s, \omega_i) = \text{sinc}[L\Delta k(\omega_r, \omega_s, \omega_i)/2] \times \exp[iL\Delta k(\omega_r, \omega_s, \omega_i)/2], \quad (9)$$

written in turn in terms of the fiber length L and the phasemismatch $\Delta k(\omega_r, \omega_s, \omega_i)$

$$\begin{aligned}\Delta k(\omega_r, \omega_s, \omega_i) &= k_p(\omega_r + \omega_s + \omega_i) - k_r(\omega_r) - k_s(\omega_s) \\ &\quad - k_i(\omega_i) + \Phi_{NL}.\end{aligned}\quad (10)$$

In Eq. (10), the last term is a non-linear contribution written as $\Phi_{NL} = [\gamma_p - 2(\gamma_{pr} + \gamma_{ps} + \gamma_{pi})]P$, where γ_p and $\gamma_{p\mu}$ are the nonlinear coefficients derived from self-phase and cross-phase modulation, respectively [21]. These coefficients may be written as

$$\gamma_p = \frac{3\chi^{(3)}\omega_{p0}}{4\epsilon_0 c^2 n_p^2 A_{eff}^{(p)}}, \quad (11)$$

and

$$\gamma_{p\mu} = \frac{3\chi^{(3)}\omega_{\mu 0}}{4\epsilon_0 c^2 n_p n_{\mu 0} A_{eff}^{(p\mu)}}, \quad (12)$$

in terms of the definition $n_{\mu 0} \equiv n_\mu(\omega_{\mu 0})$, where $\omega_{\mu 0}$ is the central frequency of the generated wave-packet ($\mu = r, s, i$). $A_{eff}^{(p)}$ and $A_{eff}^{(p\mu)}$ represent the effective interaction areas, given by $A_{eff}^{(p)} = (\int \int dxdy |A_p(x, y)|^4)^{-1}$ and $A_{eff}^{(p\mu)} = (\int \int dxdy |A_p(x, y)|^2 |A_\mu(x, y)|^2)^{-1}$, respectively. Note that these expressions for interaction areas take into account the normalization used for the transverse spatial distributions of the four modes.

III. EMITTED FLUX IN THE PROCESS OF TOSPD

In what follows, we focus on calculating the emission rate of a photon-triplet source based on the TOSPD process. In order to facilitate this calculation, we assume that pump photons are suppressed through appropriate filtering at the end of the TOSPD fiber, so that no further photon triplets are generated beyond this point. For our purposes, the source brightness is defined as the number of single photons detected in one of the three generation modes (e.g. the signal-1 mode) per unit time. For the state in Eq. (6), which assumes a pulsed pump, we are specficially interested in the number of signal-1 single photons emitted per pump pulse, N_r . An implicit assumption in this definition is that the photon triplets may be split into separate spatial modes; note that this can be achieved deterministically if the three emission modes are spectrally non-degenerate, and can be achieved only non-deterministically if the three modes are spectrally degenerate. N_r is given by

$$N_r = \sum_{k_r} \langle \Psi_3 | \hat{a}^\dagger(k_r) \hat{a}(k_r) | \Psi_3 \rangle. \quad (13)$$

Note that under ideal detection efficiency conditions, the quantity N_r also corresponds to the number of photon

triplets emitted per pump pulse. Replacing Eq. (6) in Eq. (13) it can be shown that

$$N_r = v \int dk_r \int dk_s \int dk_i \ell^2(k_r) \ell^2(k_s) \ell^2(k_i) |F(k_r, k_s, k_i)|^2, \quad (14)$$

where the parameter v is given as $v = (3)^2 |\xi|^2 / (\delta k)^3$. Note that because $|\xi|^2$ is cubic in δk , v is constant with respect to δk , and is explicitly given by

$$v = \frac{2(3)^2 (2\pi)^2 \epsilon_0^3 c^3 n_p^3}{\hbar^2 \omega_{p0}^2} \frac{\gamma^2 L^2 P}{|\int d\omega_p \alpha(\omega_p)|^2}, \quad (15)$$

where γ is the nonlinear coefficient that governs the TOSPD process, given by

$$\gamma = \frac{3\chi^{(3)}\omega_{p0}}{4\epsilon_0 c^2 n_p^2 A_{eff}}, \quad (16)$$

where A_{eff} is the effective interaction area among the four fields, expressed as

$$A_{eff} = \frac{1}{\int dx \int dy A_p(x, y) A_r^*(x, y) A_s^*(x, y) A_i^*(x, y)}. \quad (17)$$

In writing Eq. (17), we have taken into account the normalization used for the transverse spatial distribution of the four fields involved. Note that γ is distinct from γ_p and $\gamma_{p\mu}$ defined in Eqs. (11) and (12).

In calculating the signal-1-mode photon number, see Eq. (14), k -vector sums have been replaced by integrals, i.e. $\delta k \sum_k \rightarrow \int dk$, which is valid in the limit $L_Q \rightarrow \infty$.

A. Expressions for the emitted flux in integral form

We begin this section with a discussion of the pulsed-pump regime. We limit our treatment to pump fields with a Gaussian spectral envelope, which can be written in the form

$$\alpha(\omega_p) = \frac{2^{1/4}}{\pi^{1/4} \sqrt{\sigma}} e^{-\frac{(\omega_p - \omega_{p0})^2}{\sigma^2}}, \quad (18)$$

given in terms of the pump central frequency ω_{p0} and the pump bandwidth σ . The number of signal-1-mode photons N_r resulting from an isolated pump pulse can be obtained by replacing Eqns. (3), (8), (15) and (18) into Eq. (14). We further assume that the pump mode is in the form of a pulse train with a repetition rate R . Thus, the number of signal-1-mode photons generated per second is given by $N = N_r R$, from which it can be shown that

$$N = \frac{2^{5/2} 3^2 \hbar c^3 n_p^3 L^2 \gamma^2 p}{\pi^{5/2} \omega_{p0}^2 \sigma} \int d\omega_r \int d\omega_s \int d\omega_i \frac{k'_r \omega_r}{n_r^2} \times \frac{k'_s \omega_s}{n_s^2} \frac{k'_i \omega_i}{n_i^2} |f(\omega_r, \omega_s, \omega_i)|^2, \quad (19)$$

where p is the average pump power that is related to the peak pump power P through the relation $P = p\sigma/(\sqrt{2\pi}R)$. In the derivation of Eq. (19), integrals over k_r , k_s and k_i were transformed into frequency integrals through the relationship $dk_\mu = k'_\mu d\omega_\mu$, where k'_μ represents the first frequency derivative of $k(\omega)$, evaluated at ω_μ . The new function $f(\omega_r, \omega_s, \omega_i) = (\pi\sigma^2/2)^{1/4} F(\omega_r, \omega_s, \omega_i)$, is a version of the joint spectral amplitude $F(\omega_r, \omega_s, \omega_i)$ [see Eq. (8)], which does not contain factors in front of the exponential and sinc functions, so that all pre-factors terms appear explicitly in Eq. (19).

From Eq. (19) we can see that if the pump-power dependence of the phasemismatch can be neglected, the emitted flux has a linear dependence on the pump power, which implies that the conversion efficiency in the TOSPD process is constant with respect to this experimental parameter. For sufficiently large pump powers, there may be a deviation from this stated behavior, due to the pump-power dependence of the phasemismatch. The linear dependence of the emitted flux vs pump power can be directly contrasted with the corresponding behavior observed for the SFWM process, for which the emitted flux is proportional to the square of the pump power [22]. Because of this important difference, photon-triplet sources based on TOSPD are, for sufficiently high pump powers, significantly less bright than comparable SFWM sources. On the other hand, as in the case of SFWM, N varies quadratically with the nonlinear coefficient γ , which implies that the emitted flux has an inverse fourth power dependence on the transverse mode radius. The dependence of the emitted flux on other experimental parameters will be discussed in Sec. VIB.

In order to proceed with our analysis, we define the conversion efficiency as $\eta \equiv N/N_p$, where N_p is the number of pump photons per second. For a sufficiently narrow pump bandwidth, N_p is given by $N_p = U_p R/(\hbar\omega_{p0})$, with U_p the pulse energy. For a pump pulse with a spectral envelope given by Eq. (18) we obtain that

$$N_p = \frac{p}{\hbar\omega_{p0}}. \quad (20)$$

The triplet-photon conversion efficiency can then be written as

$$\eta = \frac{2^{5/2} 3^2 c^3 \hbar^2 n_p^3 L^2 \gamma^2}{(\pi)^{5/2} \omega_{p0}^2 \sigma} \int d\omega_r \int d\omega_s \int d\omega_i \frac{k'_r \omega_r}{n_r^2} \times \frac{k'_s \omega_s}{n_s^2} \frac{k'_i \omega_i}{n_i^2} |f(\omega_r, \omega_s, \omega_i)|^2. \quad (21)$$

Let us now turn our attention to the monochromatic-pump limit of the TOSPD conversion efficiency. It can be shown that by taking the $\sigma \rightarrow 0$ limit of Eq. (19), the number of photon triplets emitted per second becomes

$$N_{cw} = \frac{2^2 3^2 \hbar c^3 n_p^3 \gamma^2 L^2 p}{\pi^2 \omega_p^2} \times \int d\omega_r \int d\omega_s h(\omega_r, \omega_s, \omega_p - \omega_r - \omega_s) \times \text{sinc}^2 \left[\frac{L}{2} \Delta k_{cw}(\omega_r, \omega_s) \right], \quad (22)$$

while by taking the $\sigma \rightarrow 0$ limit of Eq. (21) the conversion efficiency becomes

$$\eta_{cw} = \frac{2^2 3^2 \hbar^2 c^3 n_p^3 \gamma^2 L^2}{\pi^2 \omega_p} \times \int d\omega_r \int d\omega_s h(\omega_r, \omega_s, \omega_p - \omega_r - \omega_s) \times \text{sinc}^2 \left[\frac{L}{2} \Delta k_{cw}(\omega_r, \omega_s) \right]. \quad (23)$$

In Eqns. (22) and (23) ω_p is the frequency of the monochromatic-pump. These equations have been written in terms of the phase mismatch $\Delta k_{cw}(\omega_r, \omega_s)$ [see Eq. (10)] defined as

$$\Delta k_{cw}(\omega_r, \omega_s) = k(\omega_p) - k(\omega_r) - k(\omega_s) - k(\omega_p - \omega_r - \omega_s) + \Phi_{NL}, \quad (24)$$

and the function $h(\omega_r, \omega_s, \omega_p - \omega_r - \omega_s)$ defined as

$$h(\omega_r, \omega_s, \omega_i) \equiv \frac{k'_r \omega_r}{n_r^2} \frac{k'_s \omega_s}{n_s^2} \frac{k'_i \omega_i}{n_i^2}. \quad (25)$$

In order to gain a better understanding of the TOSPD process, we show in the next subsection that it is possible to obtain emitted flux expressions in closed analytic form under certain approximations.

B. Non-degenerate emission frequencies: Closed analytic expressions

In order to obtain a closed analytic expression for the emitted flux, we start by considering that the function $h(\omega_r, \omega_s, \omega_i)$, contained by the integrand in Eq. (19), varies only slowly with the generation frequencies, within a sufficiently narrow spectral region of interest. Thus, in what follows we approximate this function to be constant; specifically, we evaluate the function $h(\omega_r, \omega_s, \omega_i)$ [see Eq. (25)] at the frequencies $\omega_{\mu 0}$ (where $\mu = r, s, i$), for which perfect phasematching is attained.

In addition, in order to solve the triple frequency integral in Eq. (19) we resort to a linear approximation of

the phasemismatch. Within this approximation, it can be shown that the product $L\Delta k$ in the phase matching function [see Eq. (9)] can be expressed as

$$L\Delta k_{lin} = \tau_r\nu_r + \tau_s\nu_s + \tau_i\nu_i, \quad (26)$$

written in terms of the frequency detunings $\nu_\mu = \omega_\mu - \omega_{\mu 0}$. In Eq. (26), we have assumed that the constant term of the Taylor expansion vanishes, i.e. that phase-matching is attained at the central pump and generation frequencies $\omega_{\mu 0}$ (with $\mu = p, r, s, i$). Parameters τ_μ represent group velocity mismatch coefficients between the pump and each of the emitted modes, and are given by $\tau_\mu = L(k'_{p0} - k'_{\mu 0})$, where $\mu = r, s, i$.

We also assume that before reaching the detectors, the TOSPDPC photons (in each of three modes) are transmitted through gaussian spectral filters of bandwidth $\sigma_{f\mu}$, represented by the function $f_{fil} = \exp(-\nu_\mu^2/\sigma_{f\mu}^2)$ (with $\mu = r, s, i$). The resulting filtered joint spectral amplitude function, assuming that all three filters have the same bandwidth σ_f , is given by

$$f_{fil}(\nu_r, \nu_s, \nu_i) = f(\nu_r, \nu_i, \nu_s) \exp\left[-\frac{\nu_r^2 + \nu_s^2 + \nu_i^2}{\sigma_f^2}\right]. \quad (27)$$

Then, by replacing Eqns. (25), (26), and (27) into Eq. (19) it can be shown that the number of photon triplets emitted per second is given by

$$N = \frac{3^2 \hbar c^3 n_p^3}{(2\pi)\omega_{p0}^2} \frac{L^2 \gamma^2 p \sigma_f^3}{(\sigma^2 + 3\sigma_f^2)^{1/2}} h(\omega_{r0}, \omega_{s0}, \omega_{i0}) \times \frac{1}{\Phi} \{2\sqrt{\pi} \text{Erf}[2\sqrt{\Phi}] + \exp(-4\Phi) - 1\}, \quad (28)$$

where $\text{erf}(\cdot)$ denotes the error function and Φ is given by

$$\Phi = \frac{\sigma_f^2}{32(\sigma^2 + 3\sigma_f^2)} \left[(\sigma^2 + 2\sigma_f^2)(\tau_r^2 + \tau_s^2 + \tau_i^2) - 2\sigma_f^2(\tau_r\tau_s + \tau_r\tau_i + \tau_s\tau_i) \right]. \quad (29)$$

We will concentrate our further discussion on the specific case where the filter bandwidth σ_f is much greater than the pump bandwidth σ . This scenario is realistic for a pump in the form of a picosecond-duration pulse train, as will be studied in the context of a specific example in Sec. VI. In this case, Φ reduces to $\Phi = (L/L_0)^2$, in terms of a characteristic length L_0 given by

$$L_0 = \frac{\sqrt{48}}{\sigma_f} \frac{1}{\sqrt{k_{r0}'^2 + k_{s0}'^2 + k_{i0}'^2 - k_{r0}'k_{s0}' - k_{r0}'k_{i0}' - k_{s0}'k_{i0}'}}. \quad (30)$$

Let us note that for $\sigma_f \gg \sigma$, Eq. (28) diverges for frequency-degenerate TOSDPC for which $k'_{r0} = k'_{s0} = k'_{i0}$, due to the $1/\Phi$ dependence. Indeed, the linear approximation of the phasemismatch employed here fails for frequency-degenerate TOSPDPC, unless the emission modes are strongly filtered (i.e. $\sigma_f \ll \sigma$). While the PM function $\phi(\omega_r, \omega_s, \omega_i)$ has a curvature in the emission frequencies space $\{\omega_r, \omega_s, \omega_i\}$ which limits the overlap with the PSA function $\alpha(\omega_r + \omega_s + \omega_i)$, the linearly-approximated PM function has the same orientation as the PSA function, which leads to the unphysical situation of an infinite emission bandwidth, in turn leading to the above-mentioned divergence. Thus, we restrict the use of the expression in closed analytic form for the emitted flux to the case of frequency non-degenerate TOSPDPC. As we will study in Sec. VI, our flux expression in closed analytic form for the non-degenerate case leads to excellent agreement with a numerical calculation which does not resort to approximations.

Let us now consider two different limits of Eq. (28). Note that for a sufficiently large Φ value, $[(2\sqrt{\pi}\text{Erf}[2\sqrt{\Phi}] + \exp(-4\Phi) - 1)]/\Phi$ becomes $2\sqrt{\pi}/\Phi$. Let us denote by ϕ a Φ value so that for $\Phi \gtrsim \phi$, this limit has been reached. For example, for $\Phi > 100$ which corresponds to $L > 10L_0$ the above function approaches this limit within $< 3\%$.

Thus, for $L \gtrsim \sqrt{\phi}L_0$, the number of photon triplets emitted per pump pulse can be well approximated by

$$N = \frac{6^2 \hbar c^3 k'_{r0} k'_{s0} k'_{i0}}{\sqrt{\pi} \sqrt{k_{r0}'^2 + k_{s0}'^2 + k_{i0}'^2 - k_{r0}'k_{s0}' - k_{r0}'k_{i0}' - k_{s0}'k_{i0}'}} \times \frac{\omega_{r0}\omega_{s0}\omega_{i0}}{\omega_{p0}^2} \frac{n_{p0}^3}{n_{r0}^2 n_{s0}^2 n_{i0}^2} \gamma^2 L p \sigma_f. \quad (31)$$

Conversely, for $L \lesssim \sqrt{\phi}L_0$, the number of photon triplets emitted per pump pulse becomes

$$N = \frac{18 \hbar c^3}{\sqrt{3\pi}} k'_{r0} k'_{s0} k'_{i0} \frac{\omega_{r0}\omega_{s0}\omega_{i0}}{\omega_{p0}^2} \frac{n_{p0}^3}{n_{r0}^2 n_{s0}^2 n_{i0}^2} \gamma^2 L^2 p \sigma_f^2. \quad (32)$$

Thus, while for a short fiber (compared to $\sqrt{\phi}L_0$) the flux vs fiber length is quadratic, for longer fiber lengths this dependence becomes linear. Note that L_0 represents a measure of the wavepacket length for each of the three emitted modes. Thus, the quadratic dependence appears for fibers which have a length similar or shorter as compared to the emitted wavepacket length. For most situations of interest, L_0 is a small quantity; indeed, as will be the case for the particular example studied in Sec. VI B 2, the flux dependence with fiber length can be regarded as linear, as given by Eq. (31).

This analysis serves to clarify the dependence of the emitted flux on all experimental parameters of interest, in the case of non-degenerate TOSPDPC. The emitted

flux is linear with respect to L , constant with respect to σ and linear with respect to p . Although the analytic expressions which we have obtained are not valid for frequency-degenerate TOSDPC, our numerical results (see Sec. VIB) indicate a qualitatively identical dependence of the emitted flux vs these experimental parameters.

The observed behavior for TOSDPC is different from that observed for the SFWM process, for which the emitted flux is linear in σ [22]. This means that shorter pump pulses do not lead to higher rates of emission for TOSDPC, as is the case for SFWM. Note that the manner in which the emitted flux depends on various experimental parameters is essentially identical to the behavior observed for spontaneous parametric downconversion in crystals with a second-order nonlinearity.

IV. TOSDPC PHASEMATCHING PROPOSAL

A crucial aspect in the design of a photon-triplet TOSDPC source is the need for phasematching between the four participating fields. Specifically, this translates into the condition $\Delta k(\omega_{r0}, \omega_{s0}, \omega_{i0}) = 0$ [see Eq. (10)], for a given central pump frequency.

In general, it is not trivial to fulfill phasematching for TOSDPC due to the large spectral separation between the pump and the emitted photons; for the frequency-degenerate case, pump photons at frequency 3ω are annihilated in order to generate photon triplets at ω . For most common materials including fused silica, $k(3\omega)$ is considerably larger than $3k(\omega)$, while these two quantities must be equal for the TOSDPC process operated in the low pump-power limit to be phasematched. We have proposed (see Ref. [19]) a multi-modal phasematching strategy, in which the pump mode propagates in a different fiber mode compared to the generated TOSDPC photons. Note that similar strategies have been exploited for third-harmonic generation [23, 24]. Specifically, we assume that the pump mode propagates in the first excited mode (HE_{12}), while the signal-1, signal-2, and idler photons propagate in the fundamental mode (HE_{11}) of the fiber [19]. This technique permits phasematching at the cost of limiting the attainable mode overlap between the pump and the TOSDPC modes. Furthermore, the fact that the pump must propagate in the HE_{12} mode for our phasematching strategy limits the power than can be coupled from, say, a Gaussian-transverse-distributed pump mode in free space; this will tend to limit the attainable source brightness.

We focus our attention on thin fused silica fibers guided by air, i.e. where the core is a narrow fused silica cylinder, and the cladding is the air surrounding this core. The combination of a small fiber diameter and a large core-cladding index of refraction contrast leads to a strong waveguide contribution to the overall dispersion experienced by the propagating fields which can enhance nonlinear optical effects, including TOSDPC. Note that sim-

ilar results could be obtained with photonic crystal fibers involving a large air-filling fraction in the cladding. Note also that the non-ideal TOSDPC-pump overlap observed for our multi-modal phasematching approach can to some degree be compensated by the small transverse mode area, which tends to enhance the nonlinearity γ .

In general, for a particular set of desired pump and TOSDPC frequencies, we find that a specific fiber radius can exist, to be referred to as phasematching radius, for which phasematching is attained. For optical frequencies of interest, phasematching radii tend to be in the sub-micrometer core diameter range. It is worth mentioning that such fiber radii can be obtained through current fiber taper technology (e.g. see Refs. [25–27]).

As an illustration, in Fig. 1(a) we plot as a function of the core radius the phasemismatch $k_p(3\omega) - 3k_{rsi}(\omega)$, for three different choices of the emitted frequency: $\omega = 2\pi c/1.350\mu\text{m}$, $\omega = 2\pi c/1.596\mu\text{m}$, and $\omega = 2\pi c/1.800\mu\text{m}$, where functions $k_p(\omega)$ and $k_{rsi}(\omega)$ are evaluated for the HE_{12} and HE_{11} modes, respectively. As is clear from this figure, the low-pump-power phase-matching condition $k_p(3\omega) = 3k_{rsi}(\omega)$ is fulfilled for a specific core radius for each of the considered ω values: $r = 0.331\mu\text{m}$, $r = 0.395\mu\text{m}$, and $r = 0.448\mu\text{m}$, respectively. In Fig. 1(b) we show the general trend for the degenerate TOSDPC frequency (expressed in terms of wavelength) vs phasematching radius, where the dotted vertical lines denote the specific frequencies considered in Fig. 1(a). From this figure we can see that core radii in the range 300–480nm are required for degenerate TOSDPC wavelengths within the range 1.24–1.93 μm . Note that while we have concentrated here on frequency-degenerate TOSDPC, this technique can also be extended to the frequency non-degenerate case.

In Fig. 1(b) we also show the nonlinear coefficient γ [see Eq. (16)] on the phasematching radius, for the case of frequency-degenerate TOSDPC. Note that decreasing the core radius leads to an increase in the phasematched degenerate TOSDPC frequency, and likewise to an increase in the nonlinearity γ .

V. DESIGN CONSIDERATIONS FOR PHOTON-TRIPLET SOURCES

In this section we focus on the general considerations that should be taken into account in designing a TOSDPC photon-triplet source. Of particular interest is the choice of pump and TOSDPC frequencies. For the type of fiber considered in this paper, i.e. constituted by a fused silica core and where the cladding is the air surrounding this core, the generation frequencies depend on two parameters: the fiber radius and the pump frequency. Note that while the phasemismatch has a pump-power dependence [see Eq. (10)], the overall pump-power dependence of emission frequencies tends to be negligible for pump-power levels regarded as typical.

In Fig. 2, we present a characterization of the emission

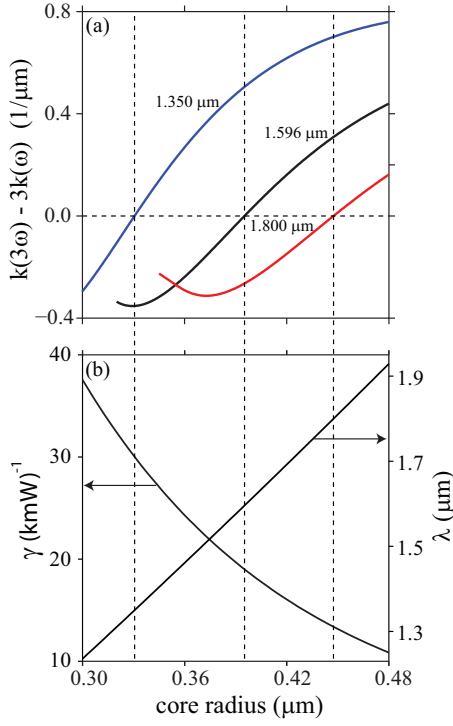


FIG. 1: (color online) (a) Frequency-degenerate phase-matching for TOSPCD at $1.350\mu\text{m}$ (blue line), $1.596\mu\text{m}$ (black line), and $1.800\mu\text{m}$ (red line). (b) Degenerate TOSPCD wavelength, and non-linear coefficient γ vs phase-matching radius.

frequencies as a function of the core radius and the pump frequency. Each of the four panels shown [(a) through (d)] corresponds to a fixed value of the idler frequency ω_i . In particular, we have chosen the following values of ω_i : (a) $\omega_i = 2\pi c/0.6\mu\text{m}$, (b) $\omega_i = 2\pi c/0.8\mu\text{m}$, (c) $\omega_i = 2\pi c/1.2\mu\text{m}$, and (d) $\omega_i = 2\pi c/1.6\mu\text{m}$. In each panel, we have plotted the phasematched signal-1(r) and signal-2(s) emission frequencies expressed as the frequency detunings $\Delta_r = \omega_r - (\omega_p - \omega_i)/2$ and $\Delta_s = \omega_s - (\omega_p - \omega_i)/2$, respectively, as a function of the pump frequency ω_p ; note that energy conservation implies that $\Delta_r = -\Delta_s$, and we define $\Delta \equiv \Delta_r$. Specifically, each curve gives combinations of pump, signal-1 and signal-2 frequencies yielding perfect phasematching, i.e. $k_p - k_r - k_s - k_i = 0$ (where we have neglected the nonlinear phase term Φ_{NL}). Different curves in a given panel were calculated for a choice of different values of the core radius (within the range $r = 0.3 - 0.5\mu\text{m}$). In all four panels, gray-shaded areas represent regions of the $\{\omega_p, \Delta_{r,s}\}$ space for which ω_r and/or ω_s lie outside of the range of validity of the dispersion relation used for fused silica. Non-physical zones for which ω_r and/or ω_s would have to be negative in order to satisfy energy conservation are shaded in black.

From these curves, it can be appreciated that for each ω_i , there is a continuum of core radii for which phase-matching occurs. For each ω_i , while the core radius can be reduced without limit and still obtain perfect phase-

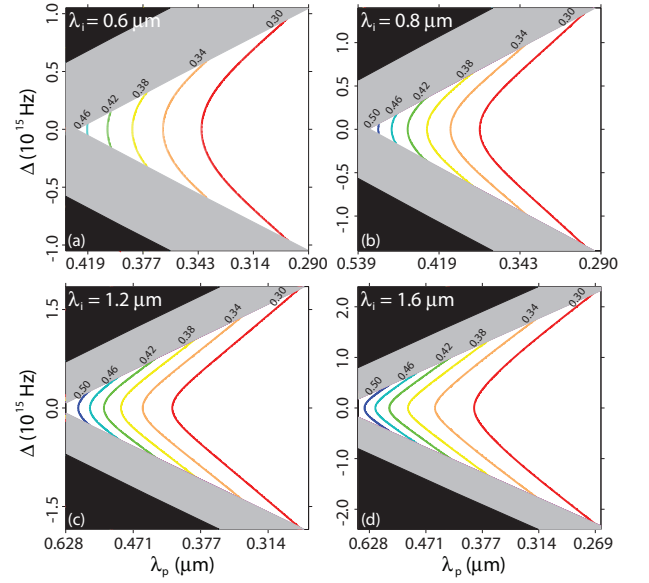


FIG. 2: (color online) Phasematched emission frequencies plotted as a function of the pump frequency, for different fiber radii, and assuming the following idler wavelengths, kept constant for each of the four panels: (a) $\lambda_i = 0.6\mu\text{m}$, (b) $\lambda_i = 0.8\mu\text{m}$, (c) $\lambda_i = 1.2\mu\text{m}$, and (d) $\lambda_i = 1.6\mu\text{m}$.

matching (within the spectral window considered here), a maximum core radius exists, above which phasematching is no longer possible. Indeed, as the core radius is increased, the spread of Δ_r and Δ_s values is reduced until it reaches the single value $\Delta_r = \Delta_s = 0$. Likewise, note that for a fixed core radius, the spread of Δ_r and Δ_s values shrinks for higher values of ω_i . Note that the vertex of the phase-matching contours indicates the emission of triplets for which $\Delta_{r,s} = 0$, or equivalently, $\omega_r = \omega_s$. Note that for a particular ω_i value, there is a single core radius for which this vertex corresponds to the frequency-degenerate emission, i.e. with $\omega_r = \omega_s = \omega_i$.

Experimental constraints such as available pump frequencies, spectral windows of single-photon detectors, and attainable fiber radii may in principle be used together with the curves in Fig. 2 in order to determine the required source parameters. An important aspect to consider is the nonlinearity γ [given by Eq. (16)], which of course has an impact on the source brightness; indeed, from Eq. (21), it is clear that the conversion efficiency scales quadratically with γ . In general, γ is determined by the core radius r , as well as by the pump and emission frequencies. In Fig. 3 we present for a fixed radius ($r = 0.395\mu\text{m}$) and a fixed idler frequency ($\omega_i = 2\pi c/1.596\mu\text{m}$) a plot of γ vs Δ and ω_p . In this figure the value of γ for each (ω_p, Δ) point is indicated by the colored background, regardless of whether or not phase matching is achieved at that point. It can be seen from this figure that significantly higher values of γ are obtained for large pump frequencies (lying in the ultra-violet region of the optical spectrum), and for $\Delta_{r,s} \rightarrow 0$ i.e., $\omega_r \rightarrow \omega_s$. The black line in Fig. 3 represents the

contour formed by phasematched frequencies. Thus, unfortunately, the highest γ values are inaccessible because they occur for unphasematched frequency combinations.

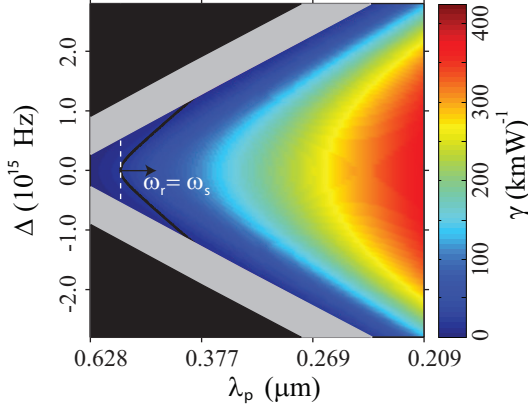


FIG. 3: (color online) Nonlinear coefficient γ as a function of ω_p and Δ , for $r = 0.395\mu\text{m}$ and $\omega_i = 2\pi c/1.596\mu\text{m}$. The black-solid line represents frequency combinations leading to perfect phasematching.

VI. SPECIFIC TOSPDG PHOTON-TRIPLET SOURCE DESIGNS

From the discussion in Sec. V, it is clear that in order to optimize the nonlinearity [see Figs. 1(b) and 3] small core radii and large pump frequencies are required. While this might suggest the use of an ultraviolet pump, in this paper we avoid the use of non-standard fiber-transmission frequencies. Thus, we propose source designs for which the pump frequency is in the region of $0.532\mu\text{m}$, which for frequency-degenerate TOSPDG results in photon triplets centered around $1.596\mu\text{m}$.

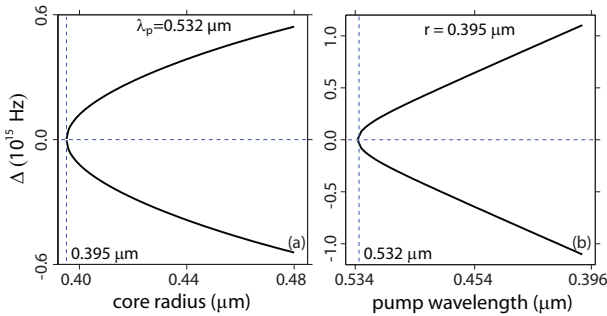


FIG. 4: (color online) (a) Phasematched emission frequencies as a function of the core radius, for a fixed pump wavelength ($\lambda_p = 0.532\mu\text{m}$). (b) Phasematched emission frequencies as a function of the pump frequency, for a fixed fiber radius ($r = 0.395\mu\text{m}$).

Let us initially assume that the pump frequency is given by $\omega_p = 2\pi c/0.532\mu\text{m}$ and let us fix the idler frequency to $\omega_i = \omega_p/3 = 2\pi c/1.596\mu\text{m}$. Fig. 4(a) shows

the resulting emission frequencies, displayed in terms of the detuning variable Δ , plotted vs the core radius r . From this figure, it is clear that there is a specific core radius ($r = 0.395\mu\text{m}$) for which the emission frequencies are characterized by $\Delta = 0$, which in this case implies $\omega_r = \omega_s = \omega_i$, i.e. for which the TOSPDG process is frequency degenerate. Note from the figure that decreasing the core radius from the value $r = 0.395\mu\text{m}$ leads to the suppression of phasematching. Likewise, note that increasing the core radius from this value, leads to $\Delta \neq 0$, so that $\omega_r = \omega_p/3 + \Delta$ and $\omega_s = \omega_p/3 - \Delta$. In other words, the three emission frequencies become distinct, leading to frequency non-degenerate TOSPDG. Thus, with a fixed pump frequency the core radius is a useful experimental parameter for the control of the degree of frequency non-degeneracy.

A similar behavior is observed by making the fiber radius, instead of ω_p , constant (to a value of $r = 0.395\mu\text{m}$), while varying ω_p . Fig. 4(b) shows the resulting emission frequencies, displayed in terms of the detuning variable Δ , plotted vs the pump frequency ω_p . From this figure, it is clear that for a pump frequency of $\omega_p = 2\pi c/0.532\mu\text{m}$, the resulting emission frequencies are characterized by $\Delta = 0$, which in this case implies frequency degenerate TOSPDG with $\omega_r = \omega_s = \omega_i$. Note from the figure that decreasing ω_p from a value of $\omega_p = 2\pi c/0.532\mu\text{m}$ leads to the suppression of phasematching. Likewise, note that increasing ω_p from this value, leads to $\Delta \neq 0$, so that $\omega_r = (\omega_p - \omega_i)/2 + \Delta$ and $\omega_s = (\omega_p - \omega_i)/2 - \Delta$. In other words, the three emission frequencies become distinct, leading to frequency non-degenerate TOSPDG. Thus, with a fixed core radius, the pump frequency is a useful experimental parameter for the control of the degree of frequency non-degeneracy.

Throughout the rest of this paper, we will consider two source designs, both based on a fiber of radius $r = 0.395\mu\text{m}$ and length $L = 10\text{cm}$.

- Frequency degenerate source, with $\omega_p = 2\pi c/0.532\mu\text{m}$ and with emission modes centered at: $\omega_r = \omega_s = \omega_i = 2\pi c/1.596\mu\text{m}$.
- Frequency non-degenerate source, with $\omega_p = 2\pi c/0.531\mu\text{m}$ and with emission modes centered at: $\omega_i = 2\pi c/1.596\mu\text{m}$, $\omega_r = 2\pi c/1.529\mu\text{m}$, and $\omega_s = 2\pi c/1.659\mu\text{m}$. As will be discussed in the next subsection, in order to guarantee that the emission modes are spectrally distinct, frequency filters should be used.

In what follows, we show plots of the joint spectral intensity function for these TOSPDG photon-triplet source designs.

A. Joint spectral intensity of the proposed TOSPDG sources

In this section, we present representations of the TOSPDG photon-triplet state for the source designs pro-

posed above. Such plots are useful in order to visualize the spectral correlations which underlie the existence of entanglement in the photon triplets.

When plotted in the generation frequencies space $\{\omega_s, \omega_r, \omega_i\}$ for typical experimental parameters, the joint spectrum of the frequency-degenerate TOSPD state is akin to a “membrane” of narrow width along the direction $\omega_s + \omega_i + \omega_r$, and much larger widths along the two perpendicular directions. In the limiting case of a monochromatic pump, this membrane becomes infinitely narrow, leading to spectrally anti-correlated photon triplets, with the sum of the three generation frequencies $\omega_s + \omega_r + \omega_i$ equal to a constant value, ω_p .

In this paper we have used two different approaches for the visualization of the JSI. On the one hand, it is useful to re-express the joint amplitude function [see Eq. (8)] in terms of frequency variables which are chosen in accordance to the symmetry exhibited by the quantum state. Thus, we use variables $\{\nu_A, \nu_B, \nu_+\}$ obtained by an appropriate rotation of the frequency detuning axes $\{\nu_r, \nu_s, \nu_i\}$ so that the new ν_A and ν_B axes are tangent to the perfect phasematching surface contour (which, again, is akin to a tilted membrane, in this case with vanishing width), and so that the ν_+ axis is normal to this surface contour. The transformation between these two sets of frequency variables is

$$\begin{aligned}\nu_+ &= \frac{1}{\sqrt{3}}(\omega_r + \omega_s + \omega_i - 3\omega_0) \\ \nu_A &= \frac{1}{2} \left(1 - \frac{1}{\sqrt{3}}\right) \omega_r + \frac{1}{2} \left(-1 - \frac{1}{\sqrt{3}}\right) \omega_s + \frac{1}{\sqrt{3}} \omega_i \\ \nu_B &= \frac{1}{2} \left(1 + \frac{1}{\sqrt{3}}\right) \omega_r + \frac{1}{2} \left(-1 + \frac{1}{\sqrt{3}}\right) \omega_s - \frac{1}{\sqrt{3}} \omega_i.\end{aligned}\quad (33)$$

We may write down a version of the joint amplitude function in terms of these new frequency variables, $f'(\nu_A, \nu_B, \nu_+)$, by expressing each of the original variables in terms of the new ones. In Fig. 5, panels (a) through (c), we have plotted the JSI function $|f'(\nu_A, \nu_B, \nu_+)|^2$ resulting from making ν_+ constant to one of three different values: -15GHz (panel c), 0 (panel b) and 15GHz (panel a), for the following choice of parameters: $L = 10\text{cm}$, $\omega_p = 2\pi c/0.532\text{nm}$, and $\sigma = 23.5\text{GHz}$ (this corresponds to one frequency-degenerate TOSPD source design). These three plots can be thought of as distinct ‘slices’ of the three-dimensional JSI at different ν_+ values. Panel (d) represents a plot of the JSI function $|f'(0, 0, \nu_+)|^2$, i.e. the choice of variables which are left constant and those that are allowed to vary are reversed. Thus, while the plot in Fig. 5(b) gives the relatively large transverse extension of the “membrane” referred to in the previous paragraph, Fig. 5(d) gives the much smaller longitudinal width of the “membrane”. From a graphical analysis of panels (a)-(c), it is clear that making ν_+ negative leads to a suppression of phasematching, while making ν_+ positive leads to a

ring structure, implying that the “membrane” referred to above is actually curved. Note that the width of the curve in Fig. 5(d) can approach zero either in the case of a very narrow pump bandwidth or in the limit of a very long fiber.

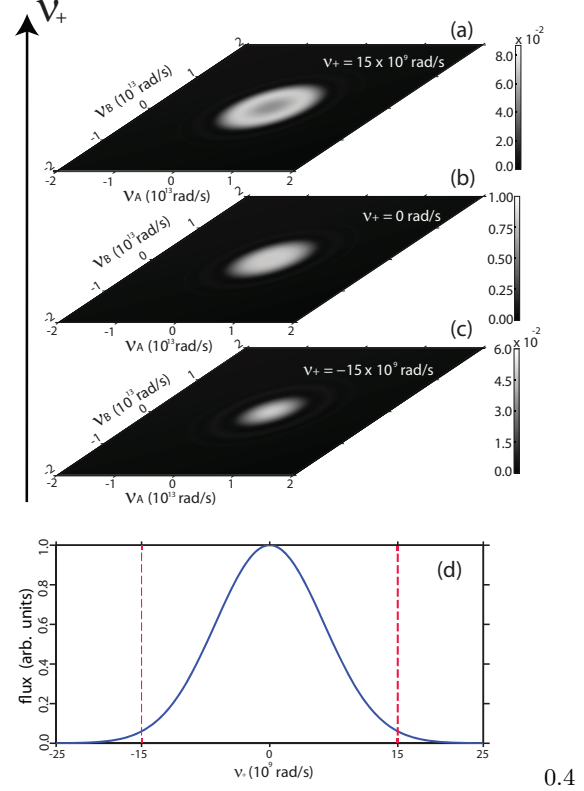


FIG. 5: (color online) Representation of the JSI for our frequency-degenerate TOSPD source design, plotted as a function of the frequency variables ν_A and ν_B for the following fixed values of ν_+ : $\nu_+ = 15 \times 10^9 \text{ rad/s}$ (a), $\nu_+ = 0$ (b) and $\nu_+ = -15 \times 10^9 \text{ rad/s}$ (c). (d) JSI plotted as a function of ν_+ , for $\nu_A = \nu_B = 0$.

It is also useful to visualize the JSI in the original $\omega_r, \omega_s, \omega_i$ variables. The structure of the JSI, again akin to a narrow, tilted membrane unfortunately makes this a difficult task. In Fig. 6 we have plotted the function resulting from making each of the JSI frequency arguments in turn equal to the degenerate frequency $\omega_p/3$, and displayed each of the three resulting plots on the corresponding plane in $\{\omega_s, \omega_r, \omega_i\}$ space. In Fig. 6, panel (a) shows a plot of the pump envelope function $|\alpha(\omega_s + \omega_r + \omega_i)|^2$ [see Eq. (18)], panel (b) shows a plot of the phase matching function $|\phi(\omega_s, \omega_r, \omega_i)|^2$ [see Eq. (9)], and panel (c) shows a plot of the JSI. Note that while the width of the phasematching function is proportional to $1/L$, the width of the pump envelope function is proportional to σ . In order to make these plots graphically clear, we have broadened each of the functions by selecting a fiber length of $L/100$ and a pump bandwidth of 200σ , where L and σ are the values assumed for our frequency-degenerate

source design. While these are not meant to constitute physically feasible values, they yield a three-dimensional appreciation of the “membrane”, except broadened, in the generation frequencies space. While in Figs. 5 and 6 we have concentrated on the frequency-degenerate source design, similar plots could be made (but are not shown here) for the frequency non-degenerate source design.

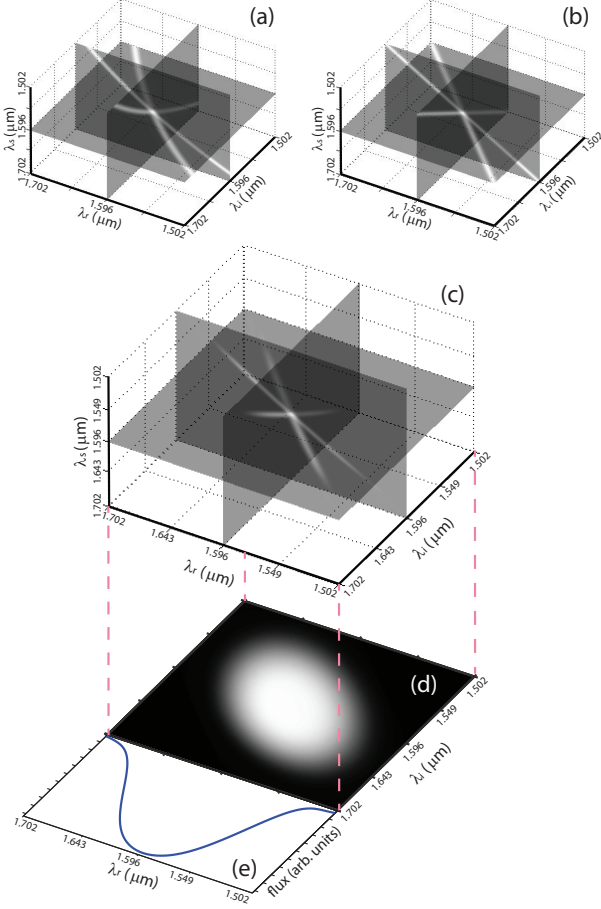


FIG. 6: (color online) Plotted as function of the three emitted frequencies $\{\omega_r, \omega_s, \omega_i\}$: (a) Phase matching function $|\phi(\omega_r, \omega_s, \omega_i)|^2$, (b) pump spectral amplitude $|\alpha(\omega_r + \omega_s + \omega_i)|^2$, and (c) JSI. (d) Two-photon spectrum $I_2(\omega_r, \omega_s)$. (e) Single-photon spectrum $I_1(\omega_r)$. Panels (a)-(c) are similar to a figure from Ref. [19].

Besides the joint spectrum $|F(\omega_r, \omega_s, \omega_i)|^2$ of the emitted photon triplets, we are also interested in the joint spectrum $I_2(\omega_r, \omega_s)$ of photon pairs resulting from disregarding one of the photons in the triplet, and in the single-photon spectrum $I_1(\omega_r)$ resulting from disregarding two of the photons in the triplet. Functions $I_2(\omega_r, \omega_s)$ and $I_1(\omega_r)$ are given by

$$I_2(\omega_r, \omega_s) = \int d\omega_i |F(\omega_r, \omega_s, \omega_i)|^2, \quad (34)$$

and

$$I_1(\omega_r) = \int d\omega_s \int d\omega_i |F(\omega_r, \omega_s, \omega_i)|^2. \quad (35)$$

Fig. 6(d) shows a plot of the two-photon joint spectrum $I_2(\omega_r, \omega_s)$ which corresponds to the three-photon joint spectrum of Fig. 6(c). Note that this two-photon joint spectrum may be informally thought of as the shadow cast, on the $\{\omega_r, \omega_s\}$ plane, by the “membrane” discussed above. Fig. 6(e) shows a plot of the single-photon spectrum $I_1(\omega_r)$ which corresponds to the three-photon joint spectrum of Fig. 6(c).

We now turn our attention to the case of frequency non-degenerate TOSPD, obtained by detuning the pump frequency while maintaining other source parameters fixed, as discussed in the context of Fig. 4(b). Let us assume that the pump frequency is $\omega_p = 2\pi c/0.531\mu\text{m}$, i.e. with a 1nm offset compared to the value assumed for the frequency-degenerate source design, above. As was studied in Fig. 4(b), for a fixed idler frequency, such a pump frequency offset leads to three distinct phase-matched frequencies for each of the three TOSPD modes: $\omega_{r0} = 2\pi c/1.529\mu\text{m}$, $\omega_{s0} = 2\pi c/1.659\mu\text{m}$, and $\omega_{i0} = 2\pi c/1.596\mu\text{m}$. However, note that for Fig. 4(b), we have arbitrarily fixed the idler frequency to the value $2\pi c/1.596\mu\text{m}$. In fact, we must consider all idler frequencies, each leading to a plot similar to Fig. 4(b) with different ω_r and ω_s values for a fixed ω_p . Thus, in order for the three emission modes to become spectrally distinct it is important to spectrally filter the idler mode, so that in this specific example only a small bandwidth centered at ω_{i0} is retained.

The 1nm offset in the pump wavelength from the previous paragraph implies that the pump envelope function intersects the phasematching function at a higher ω_+ value (compared to that for the degenerate source design) leading to a JSI which in the $\{\nu_A, \nu_B, \nu_+\}$ space is a circular ring. The two-photon JSI’s obtained by integrating the full JSI over each of the TOSPD frequencies in turn, $I_{2si}(\nu_s, \nu_i)$, $I_{2ri}(\nu_r, \nu_i)$, and $I_{2rs}(\nu_r, \nu_s)$ (where the letter subscripts indicate the corresponding TOSPD modes), then become oblong rings, as shown in Fig. 7(a)-(c).

By filtering each of the three emission modes with Gaussian spectral filters with bandwidth $\sigma_f = 15\text{THz}$ centered at each of the three selected phase-matched frequencies, ω_{r0} , ω_{s0} , and ω_{i0} , we obtain the single-photon spectra $I_{1r}(\nu)$, $I_{1s}(\nu)$, and $I_{1i}(\nu)$ (where the letter subscript indicates the corresponding TOSPD mode) shown in Figs. 7(d)-(f). Note that the spectral window transmitted by each of these filters is indicated in Fig. 7(a)-(c) by a band with lighter shading. Importantly, note that the three resulting generation modes do not overlap each other. This means that the photon triplets can then be split into three separate modes deterministically by exploiting the frequency differences among them. This is achieved, however, at the cost of a flux reduction resulting from the filters used.

In what follows, we analyze the emitted flux for our

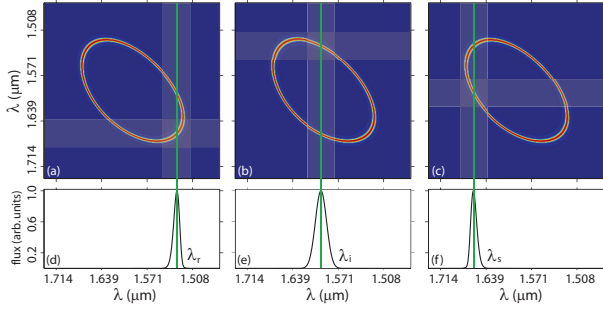


FIG. 7: (color online) Frequency non-degenerate TOSPDc photon-triplet state. (a)-(c): Two-photon spectra obtained by integrating the JSI over each of the three emission frequencies in turn. The light shaded bands indicate spectral filtering used. (d)-(f) Single photon spectra for each of the three emission modes, including the effect of spectral filtering.

two TOSPDc source designs, as a function of several key experimental parameters.

B. Emitted flux for specific TOSPDc source designs

In this section we present numerical simulations of the expected emitted flux, where possible comparing with results derived from our analytic expressions in closed form. In particular, we study the dependence of the emitted flux vs certain key experimental parameters: fiber length, pump power, and pump bandwidth. We include in this analysis our frequency-degenerate and frequency non-degenerate designs of Sec. VI, as well as the pulsed- and monochromatic-pump configurations.

We assume the following parameters: for the pulsed-pumped regime, a bandwidth of $\sigma = 23.5\text{GHz}$ (which corresponds to a Fourier-transform temporal duration of 100ps), except in Sec. VIB 1 where we analyze the emitted flux vs σ dependence; a fiber length of $L = 10\text{cm}$ except in Sec. VIB 2, where we discuss the emitted flux vs fiber length dependence; an average pump power $p = 200\text{mW}$ except in Sec. VIB 3 where analyze emitted flux vs pump power dependence.

1. Pump bandwidth dependence

In this subsection we study the dependence of the emitted flux for our two source designs on the pump bandwidth, while maintaining the energy per pump pulse constant. Note that as σ varies, the temporal duration varies, and consequently the peak power varies too. We evaluate the emitted flux for a pump bandwidth σ range $11.77 - 117.7\text{GHz}$ (or a Fourier-transform-limited temporal duration range $20 - 200\text{ps}$).

For both source designs, the emitted flux is obtained by numerical evaluation of Eq. (19). Results are shown in Fig. 8 by blue dots for the degenerate case, and by red

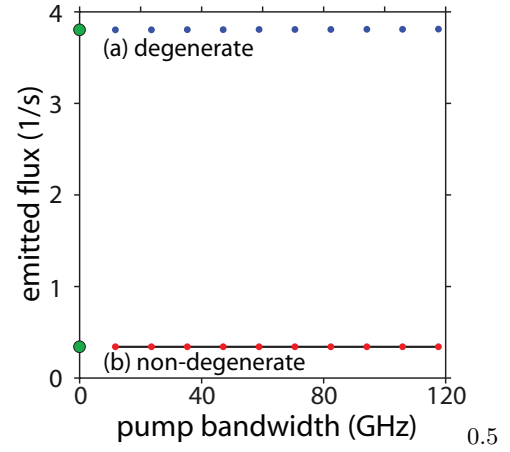


FIG. 8: (color online) Emitted flux as a function of the pump bandwidth, for the following cases: (a) Frequency-degenerate TOSPDc source, evaluated from Eq. (19) (blue dots); (b) Frequency non-degenerate TOSPDc source, evaluated from Eq. (19) (red dots), and frequency non-degenerate TOSPDc from the closed analytic expression, i.e. Eq. (28) (black solid line). Values obtained for the monochromatic pump limit, through Eq. (22), are indicated by green dots.

dots for the non-degenerate case. We have also obtained from Eq. (22) the emitted flux in the monochromatic-pump limit, shown in Fig. 8 by green dots. It is graphically clear that the emitted flux values for $\sigma \neq 0$ [calculated from Eq. (19)] approach the corresponding values in the monochromatic-pump limit [calculated from Eq. (22)]. Additionally, for our TOSPDc non-degenerate source, we evaluate the emitted flux from the analytical expression given in Eq. (28), and the corresponding results are shown in Fig. 8 by the black-solid line. As can be seen, the agreement between numerical and analytical results is excellent, indicating that the linear approximation on which the analytic results are based is in fact a good approximation. As was discussed in Sec. IIIB, this approximation fails for the frequency-degenerate case.

As is clear from Fig. 8, the TOSPDc emitted flux (and therefore the conversion efficiency) remains constant vs pump bandwidth over the full range of pump bandwidths considered, for both the degenerate and non-degenerate photon-triplet sources. For this reason, in the case of TOSPDc, no difference is expected in the emitted flux, between the monochromatic- and pulsed-pump regimes (while maintaining the average pump power constant).

Note also that the frequency-degenerate source is significantly brighter than the frequency non-degenerate source; the reason for this is that at $\omega_r = \omega_s = \omega_i = \omega_p/3$, the perfect phasematching contour and the energy conservation contour are tangent to each other, leading to a greater emission bandwidth. Our results yield a source brightness of $N = 3.80$ triplets/s for the degenerate source, and a value of $N = 0.34$ triplets/s for the non-degenerate TOSPDc source. It should be noted, however, that for the frequency-degenerate case, photon

triplets may be split only non-deterministically so that the actual usable source brightness may be lower than our results would indicate.

2. Fiber length dependence

We now turn our attention to the fiber-length dependence of the emitted flux from both the degenerate and non-degenerate TOSPDC sources, while maintaining other source parameters fixed. For this analysis we vary the fiber length from 1 to 10cm. Note that a recent experimental work shows that it is possible to obtain a uniform-radius fiber taper of $\sim 445\text{nm}$ radius over a length of 9cm [26].

The results obtained by numerical evaluation of Eq. (19) are shown in Fig. 9 by blue dots (degenerate case), and by red dots (non-degenerate case). We have also evaluated from Eq. (22) the emitted flux obtained in the monochromatic-pump limit. However, because the emitted flux is constant with respect to the pump bandwidth (for the experimental parameters assumed here), the values obtained overlap those resulting from Eq. (19), for the pulsed pump regime. Additionally, for the TOSPDC non-degenerate source, we evaluate the emitted flux from the analytical expression given in Eq. (28). The corresponding results, which are shown graphically in Fig. 9 by the black-solid line, are in excellent agreement with those obtained from Eq. (19).

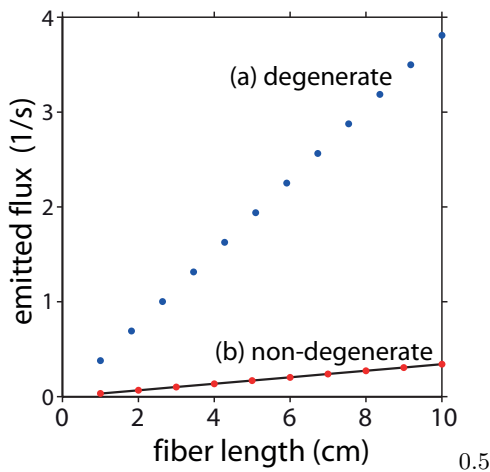


FIG. 9: (color online) Emitted flux as a function of the fiber length, for the following cases: (a) Frequency-degenerate TOSPDC source, evaluated from Eq. (19) (blue dots); (b) Frequency non-degenerate TOSPDC source, evaluated from Eq. (19) (red dots), and frequency non-degenerate TOSPDC from closed analytic expression, i.e. Eq. (28) (black solid line).

Note that for the fiber length range considered, the emitted flux exhibits a linear dependence on L for both the frequency-degenerate and the non-degenerate photon-triplet sources. However, it should be noted that there are conditions for which N has a nonlinear depen-

dence on the fiber length. For example, as it was discussed in the Sec. IIIB, for $L \ll L_0$ the emitted flux varies quadratically with the fiber length. For the longest fiber considered here ($L = 10\text{cm}$), the TOSPDC emitted flux for the degenerate source is $N = 3.80$ triplets/s and $N = 0.34$ triplets/s for the non-degenerate source.

3. Pump power dependence

We now turn our attention to the pump-power dependence of the emitted flux for the two TOSPDC sources, while maintaining the pump bandwidth and other source parameters fixed. We compute the emitted flux as a function of the average pump power, which is varied between 1 and 200 mW.

In Fig. 10 we present, for the two proposed source designs, plots of N vs p , which were obtained numerically from the expression in Eq. (19). The blue dots correspond to the degenerate case, while the red dots correspond to the non-degenerate case. Plots of the emitted flux obtained in the monochromatic-pump limit are not shown in Fig. 10, because they overlap results obtained from Eq. (19) for the pulsed-pump regime. Additionally, for our TOSPDC non-degenerate source, we evaluate the emitted flux from the analytical expression given in Eq. (28). Corresponding results are shown in Fig. 10 by the black-solid line. As can be seen, the agreement between the numerical and the analytical results is excellent.

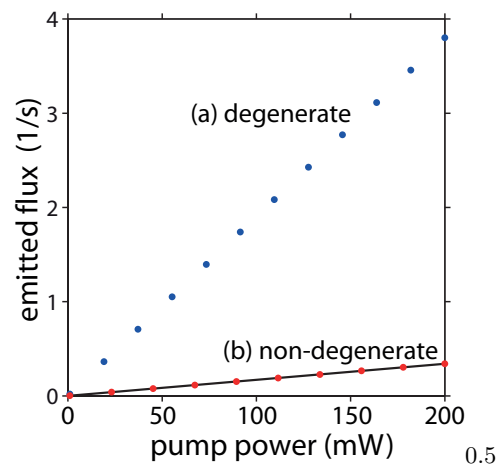


FIG. 10: (color online) Emitted flux as a function of the pump power, for the following cases: (a) Frequency-degenerate TOSPDC source, evaluated from Eq. (19) (blue dots); (b) Frequency non-degenerate TOSPDC source, evaluated from Eq. (19) (red dots), and from closed analytic expression, i.e. Eq. (28) (black solid line).

As can be seen in Fig. 10, for both sources the emitted flux depends linearly on the pump average power, which implies that the TOSPDC conversion efficiency is constant with respect to this parameter [see Eqs. (21)

and (23)]. This behavior should be contrasted with the SFWM process, for which the conversion efficiency is linear with respect to the pump power [22]. Note that the process of TOSPD has important similarities with the process of SPDC; in both cases, the conversion efficiency is constant with respect to the pump power and to the pump bandwidth (within the phasematching bandwidth).

At the highest average pump power considered here ($p = 200$ mW), the TOSPD emitted flux for the degenerate source is $N = 3.80$ triplets/s.

VII. CONCLUSIONS

In this paper we have studied the third-order spontaneous parametric downconversion process, including both the frequency-degenerate and frequency non-degenerate cases, implemented in thin optical fibers. We have based our analysis on a configuration introduced in an earlier paper from our group (see Ref. [19]), in which the pump and the generated modes propagate in different fiber modes, with the objective of attaining phasematch-

ing. In this paper we study the emitted photon-triplet TOSPD states, and present two different ways to visualize this state. We present an analysis of the photon-triplet emission flux, which leads to expressions in integral form which for frequency non-degenerate TOSPD are taken to closed analytic form under certain approximations. We show plots of the emitted flux as a function of several key parameters, obtained through numerical evaluation of our full expressions, where possible comparing with results derived from our closed analytic expressions. We also analyze the TOSPD phasematching characteristics of thin optical fibers, in particular as a function of the fiber radius and the pump frequency. We hope that this paper will be useful as the basis for the practical implementation of photon triplet sources based on third-order spontaneous parametric downconversion.

Acknowledgments

This work was supported in part by CONACYT, Mexico, by DGAPA, UNAM and by FONCICYT project 94142.

-
- [1] D. C. Burnham and D. L. Weinberg, Phys. Rev. Lett. **25**, 84, 135-179 (1970).
 - [2] M. Fiorentino, P. L. Voss, J. E. Sharping, and P. Kumar, IEEE Photonics Technol. Lett. **14**, 983 (2002).
 - [3] M. V. Chekhova, O. A. Ivanova, V. Berardi, and A. Garuccio, Phys. Rev. A **72**, 023818 (2005).
 - [4] A. A. Hnilo, Phys. Rev. A **71**, 033820 (2005).
 - [5] T. Felbinger, S. Schiller, and J. Mlynek, Phys. Rev. Lett. **80**, 492-495 (1998).
 - [6] K. Bencheikh, F. Gravier, J. Douady, A. Levenson, and B. Boulanger, C. R. Physique **8**, 206-220 (2007).
 - [7] K. Banaszek, and P. L. Knight, Phys. Rev. A **55**, 2368-2375 (1997).
 - [8] J. Douady, and B. Boulanger, Opt. Lett. **29**, 2798 (2004).
 - [9] C. Śliwa, and K. Banaszek, Phys. Rev. A **67**, 030101(R) (2003).
 - [10] C. Wagenknecht, C.-M. Li, A. Reingruber, X.-H. Bao, A. Goebel, Y.-A. Chen, Q. Zhang, K. Chen, and J.-W. Pan, Nature Photon. **4**, 549-552 (2010).
 - [11] S. Barz, G. Cronenberg, A. Zeilinger, and P. Walther, Nature Photon. **4**, 553-556 (2010).
 - [12] D. M. Greenberger, M. A. Horne, A. Shimony, and A. Zeilinger, A. J. Phys. **58**, 1131 (1990).
 - [13] D. Bouwmeester, J.-W. Pan, M. Daniell, H. Weinfurter, and A. Zeilinger, Phys. Rev. Lett. **82**, 1345-1349 (1999).
 - [14] J. Persson, T. Aichele, V. Zwiller, L. Samuelson, and O. Benson, Phys. Rev. B **69**, 233314 (2004).
 - [15] T. E. Keller, M. H. Rubin, and Y. Shih, Phys. Rev. A **57**, 2076 (1998).
 - [16] H. Hübel, D. R. Hamel, A. Fedrizzi, S. Ramelow, K.J. Resch, and T. Jennewein, Nature **466**, 601 (2010).
 - [17] D. A. Antonosyan, T. V. Gevorgyan, and G. Yu. Kryuchkyan, Phys. Rev. A **83**, 043807 (2011).
 - [18] J. G. Rarity and P. R. Tapster, Phys. Rev. A **59**, R35 (1999).
 - [19] M. Corona, K. Garay-Palmett, and A. B. U'Ren, Opt. Lett. **36**, 190-192 (2011).
 - [20] L. Mandel and E. Wolf, *Optical Coherence and Quantum Optics* (Cambridge University Press, 1995).
 - [21] G. P. Agrawal, *Nonlinear Fiber Optics*, 4th Ed. (Elsevier, 2007).
 - [22] K. Garay-Palmett, A. B. U'Ren, and R. Rangel-Rojo, Phys. Rev. A **82**, 043809 (2010).
 - [23] O. A. Kolevatova, A. N. Naumov, and A. M. Zheltikov, Laser Phys. **13**, 1040-1045 (2003).
 - [24] V. Grubsky and J. Feinberg, Optics Comm. **274**, pp. 447-450 (2007).
 - [25] L. Tong, R. G. Gattas, J. A. Ashcom, S. He, J. Lou, M. Shen, I. Maxwell and E. Mazur, Nature **426**, 816-819 (2003).
 - [26] S. Leon-Saval, T. Birks, W. Wadsworth, P. St. J. Russell, and M. Mason, Opt. Express **12**, 2864 (2004).
 - [27] G. Brambilla, J. Opt. **12**, 043001 (2010).